nature nanotechnology

LETTERS

PUBLISHED ONLINE: 10 JUNE 2012 | DOI: 10.1038/NNANO.2012.83

Self-orienting nanocubes for the assembly of plasmonic nanojunctions

Bo Gao, Gaurav Arya and Andrea R. Tao*

Plasmonic hot spots are formed when metal surfaces with high curvature are separated by nanoscale gaps and an electromagnetic field is localized within the gaps. These hot spots are responsible for phenomena such as subwavelength focusing[1,2], surface-enhanced Raman spectroscopy[3] and electromagnetic transparency[4], and depend on the geometry of the nanojunctions between the metal surfaces[5]. Direct-write techniques such as electron-beam lithography can create complex nanostructures with impressive spatial control[6] but struggle to fabricate gaps on the order of a few nanometres or manufacture arrays of nanojunctions in a scalable manner. Self-assembly methods, in contrast, can be carried out on a massively parallel scale using metal nanoparticle building blocks of specific shape[7,8]. Here, we show that polymer-grafted metal nanocubes can be self-assembled into arrays of one-dimensional strings that have well-defined interparticle orientations and tunable electromagnetic properties. The nanocubes are assembled within a polymer thin film and we observe unique superstructures derived from edge–edge or face–face interactions between the nanocubes. The assembly process is strongly dependent on parameters such as polymer chain length, rigidity or grafting density, and can be predicted by free energy calculations.

A significant challenge in the self-assembly of shaped nanoparticles is the formation of non-close-packed nanoparticle groupings that adopt specific interparticle orientations, which precludes the use of assembly methods that involve colloidal crystallization or jamming. Several strategies have been developed for achieving programmable assembly through anisotropic chemical modification of the nanoparticle surface, including the use of DNA linkers[9,10], block co-polymers[11,12] or patchy particles[13–15]. However, these approaches are solution-based, require extensive chemical modification of nanoparticle surfaces, and ultimately necessitate post-processing to transfer the nanoparticle assemblies into a dielectric material or onto a solid support.

Our approach to fabricating large-area, non-close-packed plasmonic nanoparticle arrays is to organize polymer-grafted metal nanoparticles directly within a supported polymer thin-film matrix. This multicomponent system of nanoparticles, grafted polymers and matrix polymer is expected to yield rich phase behaviour due to non-specific nanoparticle interactions arising from van der Waals and steric forces. Self-assembly can be tuned using simple parameters such as polymer chain length, graft density and miscibility. Previously, graft chain length has been demonstrated as a key parameter in dictating spherical nanoparticle assembly into anisotropic superstructures ranging from aggregates to sheets and strings[16,17]. Here, we demonstrate how graft chain length can be used to control the orientation of shaped nanoparticles within hierarchical nanojunctions. This simple yet powerful approach does not require any chemical anisotropy of the nanoparticle surface, thus simplifying surface modification and forgoing the need for face-selective surface chemistries[18]. Because assembly is not guided by strong chemical bonds between nanoparticles, our strategy allows for nanoparticle assemblies that are dynamic and can be engineered to exhibit stimulus-responsive electromagnetic behaviour. Moreover, the polymer matrix serves as a convenient dielectric medium that can be used to freeze-capture desired nanoparticle structures as they evolve.

We fabricated a 'spin-on' plasmonic film using nanoparticles organized within large-area (>6 cm^2) polystyrene thin films. The basic building block for our plasmonic layer is a metal nanocube grafted with hydrophilic polymer chains. Silver nanocubes were batch synthesized using wet chemical methods to produce colloidal dispersions of uniform particle size and shape[19,20] (see Supplementary Section S1 for full details). The cubic shape is unique in two ways. First, it is a compelling geometry for constructing non-close-packed nanoparticle architectures by coordination through facet, corner or edge sites. In the thin films fabricated here, this anisotropy leads to assembly primarily through edge–edge, face–face and face–edge orientations (Fig. 1a). Second, this shape supports the excitation of higher-order surface plasmon modes that occur through charge localization into the corners and edges of the nanoparticle. This enables orientation-dependent electromagnetic coupling between neighbouring nanoparticles[21], where interparticle junctions formed by cube corners and edges produce intense electromagnetic fields that are confined well below the conventional diffraction limit.

To induce spontaneous organization, the hydrophilic polymer-grafted nanocubes are introduced into a hydrophobic polymer matrix. In the spinodal regime[22], this immiscible blend undergoes spontaneous phase segregation to produce periodically spaced and highly aligned one-dimensional strings of nanoparticles. To maximize electromagnetic coupling within these string structures, we first targeted an edge–edge configuration by grafting the silver nanocubes with a long, floppy polymer ligand. Figure 1b shows this process for nanocubes (edge length, 80 nm) grafted with poly(vinyl pyrrolidone) (PVP, $M_w = 55{,}000$) and embedded within a polystyrene ($M_w = 10{,}900$) thin film with a thickness of 150 nm. As the film is annealed using thermal or solvent vapour treatment, the nanoparticles assemble in the edge–edge configuration to form strings that continuously grow and converge (Fig. 1c–e). The formation of strings is likely to result from two effects: large steric repulsion due to an effective increase in graft density locally at nanojunction sites[23], and diffusion-limited assembly resulting from low nanoparticle mobility within the viscous polymer matrix[24]. However, these mechanisms for long-range order operate independently of the short-range interparticle interactions that give rise to specific nanocube orientations within an assembled nanojunction.

To provide insights into the experimental parameters that dictate the orientation of our nanocubes, we performed Monte Carlo simulations of polymer-grafted nanocubes treated at a coarse-grained resolution (see Supplementary Section S3 for full details of the computational methods). Our approach computes the potential of mean

NanoEngineering Department, University of California, San Diego, La Jolla, California 92093-0448, USA. *e-mail: atao@ucsd.edu

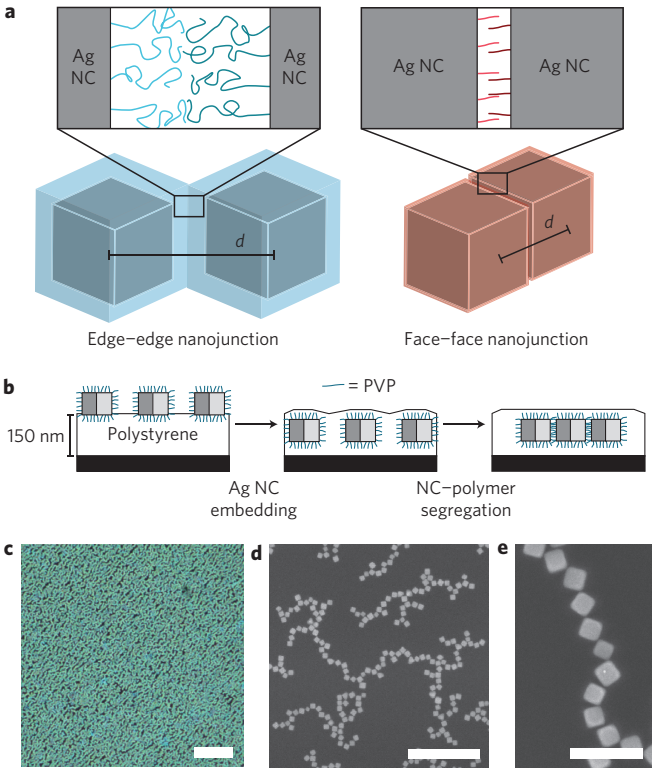

Figure 1 | Self-oriented nanocrystals for plasmonic materials. a, Schematic of assembly of silver nanocubes (NCs) into edge-edge and face-face orientations by modifying the surface of the nanocubes with polymer grafts of different chain lengths. **b**, Schematic of the assembly process for edge-edge nanojunctions. During the solvent annealing process, PVP-grafted nanocubes are embedded into a polystyrene thin film. The nanoparticle-polymer composite then undergoes spontaneous phase segregation to form nanocube strings. **c**, Nanocube strings assemble uniformly across the entire film as observed by dark-field optical microscopy. The texture observed in this image results from individual nanocube strings (green areas) distributed within the polymer matrix (black areas), but resolution is limited by the diffraction limit. Variations in colour are derived from strings with different lengths and branching structures. Scale bar, 10 μm. **d**,**e**, SEM images of the edge-edge-oriented nanocubes within the polystyrene matrix. Scale bars, 1 μm (**d**) and 200 nm (**e**).

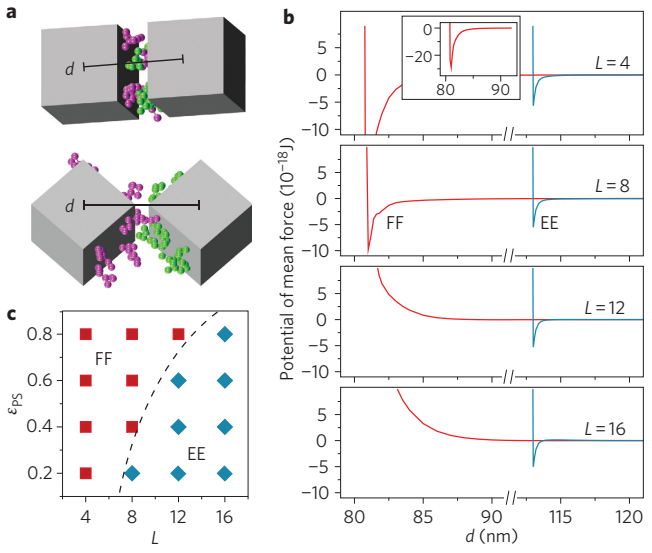

Figure 2 | Theoretically predicted interaction between silver nanocubes. **a**, Representative snapshots of face-face- and edge-edge-oriented nanocubes grafted with polymer chains of length $L = 8$ beads. Chains on the two nanocubes are coloured differently for clarity. **b**, Computed potential of mean forces W for face-face (FF, blue lines) and edge-edge (EE, red lines) oriented nanocubes grafted with varying chain lengths L and fixed polymer-surface interaction strength ($\varepsilon_{PS} = 0.4$) plotted as a function of the centre-to-centre separation distance d. The inset for $L = 4$ depicts the entire energy well that occurs for the face-face configuration, which is significantly deeper than for the other calculated chain lengths. **c**, Phase diagram showing the most favourable nanocube orientation for varying L and ε_{PS}, as predicted from our PMF calculations. The dashed line symbolizes the boundary between the face-face and edge-edge phases.

force (PMF) between two nanocubes oriented in the face–face and edge–edge configurations as a function of their centre-to-centre separation distance d (Fig. 2a). The PMF, which gives the free energy of interaction between nanocubes, allows us to determine the most favourable orientation and equilibrium separation distance between two cubes. We examined the effects of varying the length L of the grafted polymer chains and the effective strength of attraction ε_{PS} with the nanocube surface. Other system parameters did not produce an appreciable effect on the interactions between the nanocubes (such as grafted polymer interaction, ε_{PP}) or are difficult to tune experimentally (such as matrix polymer interactions). Figure 2b shows the computed PMF of two nanocubes in face–face (red line) and edge–edge (blue line) orientations grafted with polymer chains of varying length L as a function of separation distance d. When the grafted chains are short ($L \leq 4$ monomer units), it is energetically favourable for the nanocubes to orient in the face–face configuration. The face–face-oriented nanocubes exhibit a strong van der Waals attraction that exceeds the steric repulsion between chains, yielding a deep energy minimum (Supplementary Fig. S4a). In contrast, the edge–edge-oriented nanocubes exhibit a weak van der Waals attraction and negligible steric repulsion, yielding a shallower energy minimum compared with the face–face arrangement (Supplementary Fig. S4b). When the polymers grafted to the nanocubes are long, the edge–edge configuration now becomes more energetically favourable. This is because the steric repulsion between these longer polymer chains exceeds the van der Waals attraction in the face–face-oriented nanocubes, making the net free energy repulsive (Supplementary Fig. S4c). In contrast, the edge–edge-oriented nanocubes still exhibit weak steric repulsion and van der Waals attraction, leading to a moderate but net attractive free energy profile (Supplementary Fig. S4d).

The interactions between grafted chains and the nanocube surface also play an important role in establishing the most favourable nanocube orientation. When the effective energy parameter between the polymer chains and the metal surface (ε_{PS}) is small, the edge–edge configuration becomes more energetically favourable with increasing polymer chain length compared with the face–face configuration. When ε_{PS} is strong, this transition occurs at longer L (Supplementary Fig. S5). This result can be intuitively understood by considering that the face–face configuration allows for significantly more favourable polymer–surface contacts than the edge–edge configuration. This interplay between chain length and polymer–surface interactions gives rise to the assembly phase diagram of Fig. 2c, which summarizes the favoured orientation of the nanocubes over a broad range of L and ε_{PS}.

To demonstrate that this phase diagram can be used to tailor nanoparticle orientation, we induced the rearrangement of polymer-embedded cubes from the edge–edge to the face–face configuration. We chose to focus on tuning polymer chain length L, which can be explicitly dictated by the choice of nanoparticle ligand and where ligand binding to metal nanoparticles can be accomplished using simple thiol chemistry. The face–face

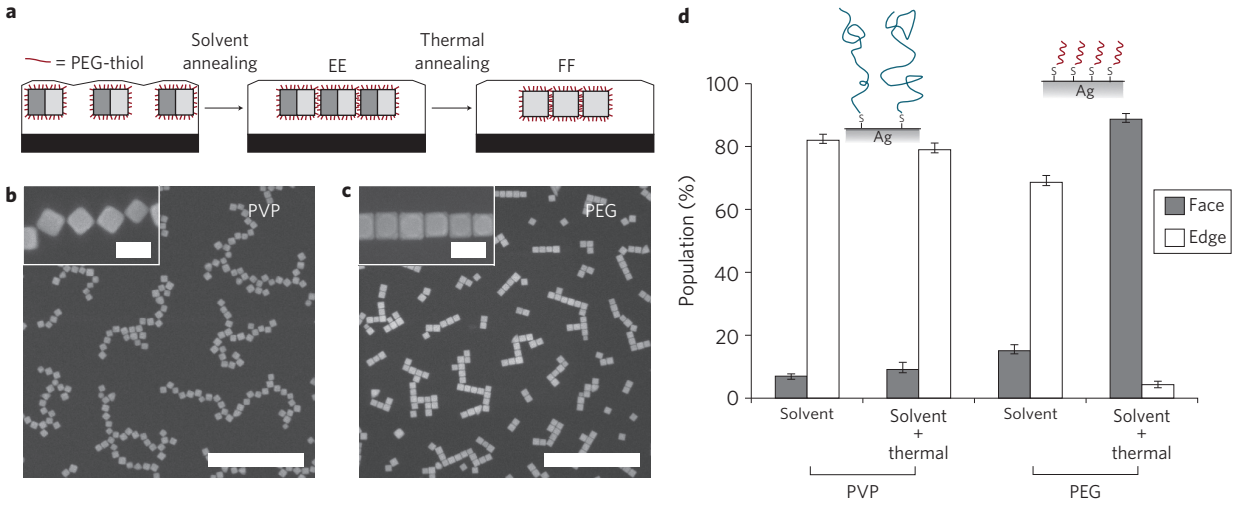

Figure 3 | Chain-length-dependent orientation of nanocube junctions. a, Schematic of the assembly of PEG-grafted nanocubes. On thermal annealing, the nanocubes rearrange from the edge–edge (EE) to face–face (FF) configuration. **b**,**c**, SEM images of nanocubes modified with PVP-thiol after solvent annealing (**b**) and PEG-alkanethiol ligands after both solvent annealing and thermal annealing at $T > T_g$ for 4 h (**c**). On thermal treatment, the PEG-modified nanocubes are converted to assemblies formed through face coordination. Scale bars (**b**,**c**), 1 μm; inset scale bars (**b**,**c**,), 100 nm. **d**, Per cent of edge and face coordination in nanocube assemblies before and after thermal treatment. Nanocubes modified with PVP experience little to no change in orientation, whereas nanocubes modified with PEG experience almost complete orientation rearrangement.

orientation requires nanoparticle grafts that are rigid and have relatively short chains. We chose to modify the silver surface with (11-mercaptoundecyl)tetra(ethylene glycol), an alkanethiol terminated with a four-monomer polyethylene glycol (PEG) chain. (See Supplementary Section S4 for full details of surface modification.) These grafts are expected to form a densely packed molecular monolayer, but still allow interdigitation between the matrix polymer and the PEG moieties. As a control, we tested nanocubes chemically modified with thiol-terminated PVP ($M_w = 1{,}700$). Based on monomer unit persistence lengths, we estimate that the PEG chains have an end-to-end distance of 2.0 nm (ref. 25), in comparison to PVP chains, which exhibit a length of 5.7 nm. Our Monte Carlo simulations predict that the PEG-modified cubes will adopt the edge–edge configuration at large interparticle distances and will reorient to adopt the face–face configuration at a shorter, critical distance (Fig. 2b, top plots). To prevent cubes from becoming kinetically trapped in edge–edge assemblies—which represents a local free energy minimum but not the global minimum—films were subjected to a two-step annealing process, first by exposure to chloroform vapour, resulting in the formation of edge–edge assemblies, and second by thermal treatment above T_g of the polystyrene matrix to rearrange these assemblies into the face–face configuration (Fig. 3a). Figure 3b,c presents scanning electron microscope (SEM) images of plasmonic films containing PVP- and PEG-grafted nanocubes, respectively. Before thermal treatment, $15.1 \pm 1.9\%$ of PEG-grafted cubes are in the face–face orientation and $68.6 \pm 2.2\%$ are in either the edge–edge or face–edge orientations (Supplementary Fig. S8). After thermal treatment, the particles remain assembled in one-dimensional domains but with $88.7 \pm 1.8\%$ of the particles oriented in the face–face configuration (Fig. 3d). When grafted with the short PEG chains, thermal activation is able to overcome the energy barrier for cube rotation from the edge–edge to the face–face configuration. As confirmation, face–face assembly is not observed without PEG modification or without thermal activation of the nanocube–polymer film.

Additional assembly experiments using long ($M_w = 5{,}000$) and extra-long ($M_w = 54{,}000$) PEG grafts were carried out to confirm the effect of chain length and to rule out the contribution of specific chemical interactions in this reorientation. The use of extra-long PEG grafts resulted in nanocube assemblies with a large percentage of edge–edge-oriented nanojunctions. However, we observed defects attributed to partial dewetting of the matrix polymer near the cube surface on solvent vapour exposure. Extra-long PEG grafts tend to collapse into globular structures, which may contribute to the poor interaction between the graft and the matrix polymer. This was ameliorated by using long PEG grafts with a lower molecular weight and by thermal annealing to promote polymer redistribution. Nanocubes modified with these long-chain PEG grafts assemble predominantly in the edge–edge configuration and remain in the edge–edge configuration after extended periods of thermal treatment (see Supplementary Section S7 for the details of these results).

The surface plasmon modes supported by nanoparticle–polymer films in these two nanojunction orientations are expected to produce different field localization effects, as predicted by electrodynamic simulations for nanocube dimers (Fig. 4a). This orientation dependence may provide a convenient strategy for tuning the optical properties of the large-scale films (Fig. 4b) or the surface plasmon coupling properties of individual nanoparticle strings. To probe this experimentally, we measured the optical extinction spectra for films containing PVP-grafted nanocubes oriented in the edge–edge configuration and PEG-grafted nanocubes in the face–face configuration. The optical response of each film changes dynamically with increased annealing time as the nanoparticles assemble and form longer string structures (Fig. 4c,d). String length was tuned by varying the solvent exposure times for each sample, and a detailed analysis of string length is given in Supplementary Table S2. Optical spectra were collected by measuring the transmission of unpolarized light over a sample area of 0.8 cm^2 to demonstrate the uniformity of nanoparticle orientation across a macroscopic area.

Compared with the plasmon response generated by isolated nanocubes before assembly (Supplementary Fig. S9), both films exhibit scattering peaks at $\lambda > 600$ nm attributed to strong electromagnetic coupling and the generation of new coupled surface plasmon modes from assembled nanoparticles. Although we observe that these peaks are quite broad (which we attribute to non-uniform string branching), these modes become more intense as the strings grow in length. In the edge–edge configuration, we observe that

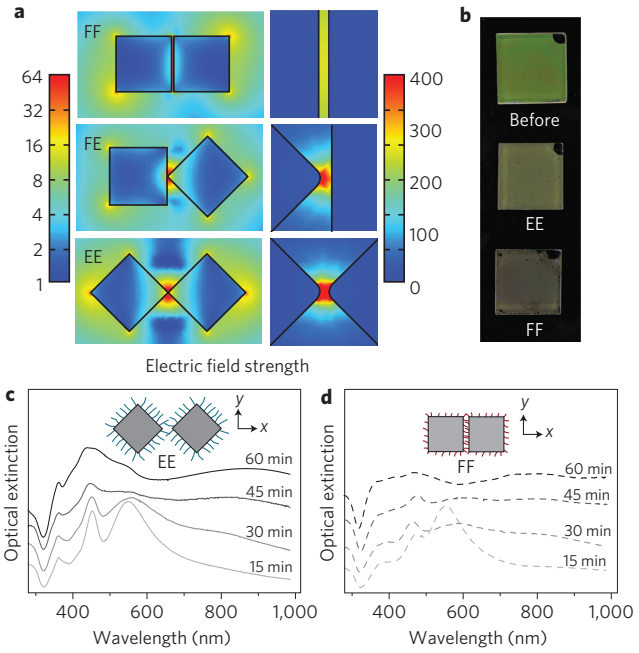

Figure 4 | Plasmonic response of the oriented nanojunctions. a, Electric field strength (colour scale) for silver nanocubes with edge lengths of 80 nm and a separation gap of 2 nm in three favoured orientations: face-face (FF), face-edge (FE) and edge-edge (EE). Field strengths are plotted in units of $V\,m^{-1}$ for an incident field of $E_o = 1\ V\,m^{-1}$. Cross-sections are taken in the *x*-*y* plane bisecting the nanocubes. Field distributions are shown for excitation wavelengths of 750 nm (face-face), 670 nm (face-edge) and 670 nm (edge-edge) corresponding to the coupled surface plasmon mode for each of the nanocube dimers. For visual contrast, the electric field strength is plotted on a $\log_2$ scale with min/max cutoffs as shown in the colour legend. Magnified regions of the nanojunctions are shown in the images on the right, which correspond to an area of 20 nm × 20 nm. For visual contrast, the electric field strength is plotted with min/max cutoffs as shown in the colour legend. The edge-edge configuration supports the strongest field localization in the narrow interparticle gap, with a maximum field enhancement of $>800E_o$ in the gap centre and $>1{,}200E_o$ at the nanocube corners. **b**, Digital camera images of films covering a quartz substrate of area ~5 cm^2 with embedded but unassembled nanocubes (Before), edge-edge-oriented nanocubes (EE) and face-face-oriented nanocubes (FF). **c**,**d**, Measured extinction spectra of nanocomposite films containing PVP-grafted nanocubes in the edge-edge orientation (**c**) and PEG-grafted nanocubes in the face-face orientation (**d**). Films in both orientations show peaks corresponding to coupled surface plasmon modes in the near-infrared. Spectra were taken for samples subjected to different solvent vapour exposure times to obtain films with varying nanoparticle string lengths: 15 min (one particle), 30 min (two particles), 45 min (six particles) and 60 min (15+ particles). For the spectra in **d**, films were subjected to an additional thermal annealing step to switch the edge-edge-oriented strings to face-face-oriented strings. Detailed analysis of string length and representative SEM images are provided in the Supplementary Information.

plasmonic coupling results in a long-wavelength surface plasmon that redshifts (from 776 nm to 895 nm) as string length increases. Our simulations for edge–edge-oriented strings indicate that maximum field localization occurs in the interstitial junction between nanocube edges (Supplementary Fig. S10). In contrast, nanocubes assembled in the face–face configuration behave increasingly like broadband scatterers as string length is increased. This behaviour probably results from surface plasmon delocalization along the extended nanoparticle string, as indicated by simulations showing regions of maximum field localization smeared over the boundaries of the string. Looking ahead, further tuning of ε_{PS} should be able to provide control over string branching and curvature, with the potential to form plasmon-based interconnects or waveguide structures with spatial complexities that are not achievable through top-down approaches.

We demonstrate the self-assembly of shaped nanoparticles into non-close-packed arrangements with engineered interparticle junctions. The scalability and ease of fabrication of our approach is valuable to research aimed at the discovery and application of novel plasmonic superstructures. The current limitation of our polymer-mediated assembly is achieving exact nanoparticle groupings. Our nanocube strings exhibit a distribution of string lengths, in part due to branching. It will be necessary to obtain better kinetic control over the segregation process to achieve precise nanoparticle groupings that can rival current lithographically fabricated patterns. This may be achieved through nanoparticle pinning or by making use of multipolymer blends or block co-polymer matrices to confine microphase segregation to smaller domains. Complementary polymer patterning techniques[26] may also be used to direct nanoparticle assembly into superstructures that exhibit more complex curvature, such as split-rings[27] or three-dimensional assemblies[28]. These techniques have the potential for generating spin-on optical nanocircuits[29], fully addressable plasmonic elements or metamaterial coatings[30] and for achieving more complex nanoarchitectures.

Received 7 October 2011; accepted 27 April 2012; published online 10 June 2012

References

1. Barnes, W. L., Dereux, A. & Ebbesen, T. W. Surface plasmon subwavelength optics. *Nature* **424,** 824–830 (2003).
2. Ghosh, S. K. & Pal, T. Interparticle coupling effect on the surface plasmon resonance of gold nanoparticles: from theory to applications. *Chem. Rev.* **107,** 4797–4862 (2007).
3. Hyunhyub, K., Srikanth, S. & Vladimir, V. T. Nanostructured surfaces and assemblies as SERS media. *Small* **4,** 1576–1599 (2008).
4. Fan, J. A. *et al.* Self-assembled plasmonic nanoparticle clusters. *Science* **328,** 1135–1138 (2010).
5. Stebe, K. J., Lewandowski, E. & Ghosh, M. Oriented assembly of metamaterials. *Science* **325,** 159–160 (2009).
6. Gramotnev, D. K. & Bozhevolnyi, S. I. Plasmonics beyond the diffraction limit. *Nature Photon.* **4,** 83–91 (2010).
7. Nie, Z., Petukhova, A. & Kumacheva, E. Properties and emerging applications of self-assembled structures made from inorganic nanoparticles. *Nature Nanotech.* **5,** 15–25 (2009).
8. Whitesides, G. M. & Grzybowski, B. Self-assembly at all scales. *Science* **295,** 2418–2421 (2002).
9. Xu, X., Rosi, N. L., Wang, Y., Huo, F. & Mirkin, C. A. Asymmetric functionalization of gold nanoparticles with oligonucleotides. *J. Am. Chem. Soc.* **128,** 9286–9287 (2006).
10. Millstone, J. E. *et al.* DNA–gold triangular nanoprism conjugates. *Small* **4,** 2176–2180 (2008).
11. Lin, Y. *et al.* Self-directed self-assembly of nanoparticle/copolymer mixtures. *Nature* **434,** 55–59 (2005).
12. Shenhar, R., Norsten, T. B. & Rotello, V. M. Polymer-mediated nanoparticle assembly: structural control and applications. *Adv. Mater.* **17,** 657–669 (2005).
13. Caswell, K. K., Wilson, J. N., Bunz, U. H. F. & Murphy, C. J. Preferential end-to-end assembly of gold nanorods by biotin–streptavidin connectors. *J. Am. Chem. Soc.* **125,** 13914–13915 (2003).
14. DeVries, G. A. *et al.* Divalent metal nanoparticles. *Science* **315,** 358–361 (2007).
15. Nie, Z. *et al.* Self-assembly of metal–polymer analogues of amphiphilic triblock copolymers. *Nature Mater.* **6,** 609–614 (2007).
16. Akcora, P. *et al.* Anisotropic self-assembly of spherical polymer-grafted nanoparticles. *Nature Mater.* **8,** 354–359 (2009).
17. Maillard, D., Kumar, S. K., Rungta, A., Benicewicz, B. C. & Prud'homme, R. E. Polymer-grafted-nanoparticle surfactants. *Nano Lett.* **11,** 4569–4573 (2011).
18. Glotzer, S. C. & Solomon, M. J. Anisotropy of building blocks and their assembly into complex structures. *Nature Mater.* **6,** 557–562 (2007).
19. Sun, Y. & Xia, Y. Shape-controlled synthesis of gold and silver nanoparticles. *Science* **298,** 2176–2179 (2002).
20. Tao, A., Sinsermsuksakul, P. & Yang, P. Polyhedral silver nanocrystals with distinct scattering signatures. *Angew. Chem. Int. Ed.* **45,** 4597–4601 (2006).
21. Lee, S. Y. *et al.* Dispersion in the SERS enhancement with silver nanocube dimers. *ACS Nano* **4,** 5763–5772 (2010).

22. Bates, F. S. Polymer–polymer phase behavior. *Science* **251,** 898–905 (1991).
23. Pryamtisyn, V., Ganesan, V., Panagiotopoulos, A. Z., Liu, H. & Kumar, S. K. Modeling the anisotropic self-assembly of spherical polymer-grafted nanoparticles. *J. Chem. Phys.* **131,** 221102 (2009).
24. Li, L. *et al.* Kinetically trapped co-continuous polymer morphologies through intraphase gelation of nanoparticles. *Nano Lett.* **11,** 1997–2003 (2011).
25. Zhu, B., Eurell, T., Gunawan, R. & Leckband, D. Chain-length dependence of the protein and cell resistance of oligo(ethylene glycol)-terminated self-assembled monolayers on gold. *J. Biomed. Mater. Res.* **56,** 406–416 (2001).
26. Nie, Z. & Kumacheva, E. Patterning surfaces with functional polymers. *Nature Mater.* **7,** 277–290 (2008).
27. Kanté, B., de Lustrac, A., Lourtioz, J-M. & Gadot, F. Engineering resonances in infrared metamaterials. *Opt. Express* **16,** 6774–6784 (2008).
28. Agarwal, U. & Escobedo, F. A. Mesophase behaviour of polyhedral particles. *Nature Mater.* **10,** 230–235 (2011).
29. Engheta, N. Circuits with light at nanoscales: optical nanocircuits inspired by metamaterials. *Science* **317,** 1698–1702 (2007).
30. Xiao, S., Chettiar, U. K., Kildishev, A. V., Drachev, V. P. & Shalaev, V. M. Yellow-light negative-index metamaterials. *Opt. Lett.* **34,** 3478–3480 (2009).

Acknowledgements

A.R.T. acknowledges financial support from UCSD start-up funds, a NSF BRIGE grant (ECCS-1125789) and a Hellman Fellowship.

Author contributions

B.G. and A.R.T. conceived and designed the assembly experiments. B.G. performed the assembly experiments. G.A. designed and performed Monte Carlo calculations. A.R.T. performed finite element method simulations. G.A. and A.R.T. co-wrote the paper.

Additional information

The authors declare no competing financial interests. Supplementary information accompanies this paper at www.nature.com/naturenanotechnology. Reprints and permission information is available online at http://www.nature.com/reprints. Correspondence and requests for materials should be addressed to A.R.T.